HEALTH AND MEDICINE

Design and tuning of ionic liquid–based HNO donor through intramolecular hydrogen bond for efficient inhibition of tumor growth

Xiaoyu Lv[1]*, Kaihong Chen[1]*, Guiling Shi[1], Wenjun Lin[1], Hongzhen Bai[1†], Haoran Li[1], Guping Tang[1], Congmin Wang[1,2†]

Developing ionic liquid (IL) drugs broaden new horizons in pharmaceuticals. The tunable nature endows ILs with capacity to delivery active ingredients. However, the tunability is limited to screen ionic components, and none realizes the kinetic tuning of drug release, which is a key challenge in the design of IL drugs. Here, a series of ILs are developed using biocompatible ionic components, which realizes absorption of gaseous NO to yield IL-NONOates. These IL-NONOates serve as HNO donors to release active ingredient. The release kinetics can be tuned through configuring the geometric construction of ILs (release half-lives, 4.2 to 1061 min). Mechanism research indicates that the tunability depends on the strength of intramolecular hydrogen bond. Furthermore, the IL-based HNO donors exert pharmacological potential to inhibit tumor progression by regulating intratumoral redox state. Coupled with biosafety, these IL-based HNO donors with facile preparation and tunable functionalization can be promising candidates for pharmaceutical application.

INTRODUCTION

Ionic liquids (ILs), defined as organic salts composed of cations and anions with a melting point below 100°C, have increasingly attracted attentions in chemical synthesis, catalysts, separation, electrochemistry, analytics, etc., because of their unique physical properties, such as extremely low vapor pressure, wide liquid temperature range, nonflammability, and high thermal and chemical stability (*1*–*10*). Recently, developing IL drugs has paved a new realm of pharmaceutical research owing to the superiorities of ILs in solubility, absorbability, and stability. Although works have proven ILs as ideal drug candidates for delivering active pharmaceutical ingredients (termed as API-ILs), there is still a long way for IL drugs to meet the requirement of pharmaceuticals (*11*–*16*). One crucial challenge is to realize the tunability for IL drugs, by which the release kinetics of IL drugs can be regulated to improve the bioavailability for APIs. However, to the best of our knowledge, the tunability of IL drugs is usually limited to screen ionic components with low toxicity, excellent solubility, and high absorbability, and few works have focused on tuning the drug release kinetics by exploiting the chemical motifs of ILs (*11*). Moreover, our previous studies have demonstrated that the ILs are reversible and tunable materials for gas capture, and it would be interesting to develop new IL drugs that contain gaseous active ingredients and exert a desirable drug release profile for pharmacological application.

Nitric oxide (NO) is a unique bioactive molecule in many biological processes such as cardiovascular, nervous, and immune systems, which earned Furchgott, Ignarro, and Murad the 1998 Nobel Prize in physiology or medicine (*17*–*21*). Nitroxy (HNO), one electron reduced and protonated from NO, has aroused great interest in oncology (*22*, *23*). HNO has been found to inhibit the activity of thiol-containing enzymes (including aldehyde dehydrogenase and glyceraldehyde 3-phosphate dehydrogenase), which are key regulators of proliferation and protection of cancer cells (*24*). This bioactivity of HNO makes the HNO donors (molecules that can release HNO) find an important place within the therapeutic arsenal against cancer. Several HNO donors such as Angeli's salt (AS) and Piloty's acid have been applied in the investigations of tumor inhibition (*25*–*27*). AS ($Na_2N_2O_3$) is a class of O-bound diazeniumdiolates (termed as NONOates). Of another special interest to us is N-bound diazeniumdiolates, a famous class of NO or HNO donors (*28*, *29*). These compounds can release corresponding products in physiological buffer, which can be monitored easily with ultraviolet-visible (UV-vis) spectroscopy, but the released product varies from different structures: NONOates derived from secondary amine will release NO, while primary analogs predominantly release HNO (*20*). In addition to final products, the release kinetic is another key parameter to the biological effect of HNO donor. AS and Piloty's acid exert rapid release with short half-lives ($t_{1/2}$), which may obstruct their therapeutic effects (*25*, *26*).

Here, we present an interesting strategy to develop a series of newly designed IL-based HNO donors. First, a class of amino-functionalized ILs was engineered by screening the biocompatible ionic components. These ILs were designed to capture atmospheric NO under mild conditions to yield IL-NONOates. Second, IL-NONOates could be chemically tuned by configuring intramolecular hydrogen bonds, achieving a sustained HNO release for pharmacological application. Third, in vitro and in vivo studies were conducted for these IL-NONOates to demonstrate their pharmacological potential in tumor inhibition. Our study indicated that these IL-NONOates exerted sustained HNO release under physiological conditions and effectively regulated intratumoral redox state (Fig. 1A). This regulation further inhibited the tumor progression. Quantum chemical calculation and spectroscopic investigation proved that the sustained HNO release from IL-NONOates was attributed to the intramolecular hydrogen bond, which showed obvious distinction and innovation as compared to existing HNO donors.

[1]Department of Chemistry, ZJU-NHU United R&D Center, Zhejiang University, Hangzhou 310027, China. [2]Key Laboratory of Biomass Chemical Engineering of Ministry of Education, Zhejiang University, Hangzhou 310027, China.
*These authors contributed equally to this work.
†Corresponding author. Email: hongzhen_bai@zju.edu.cn (H.B.); chewcm@zju.edu.cn (C.W.)

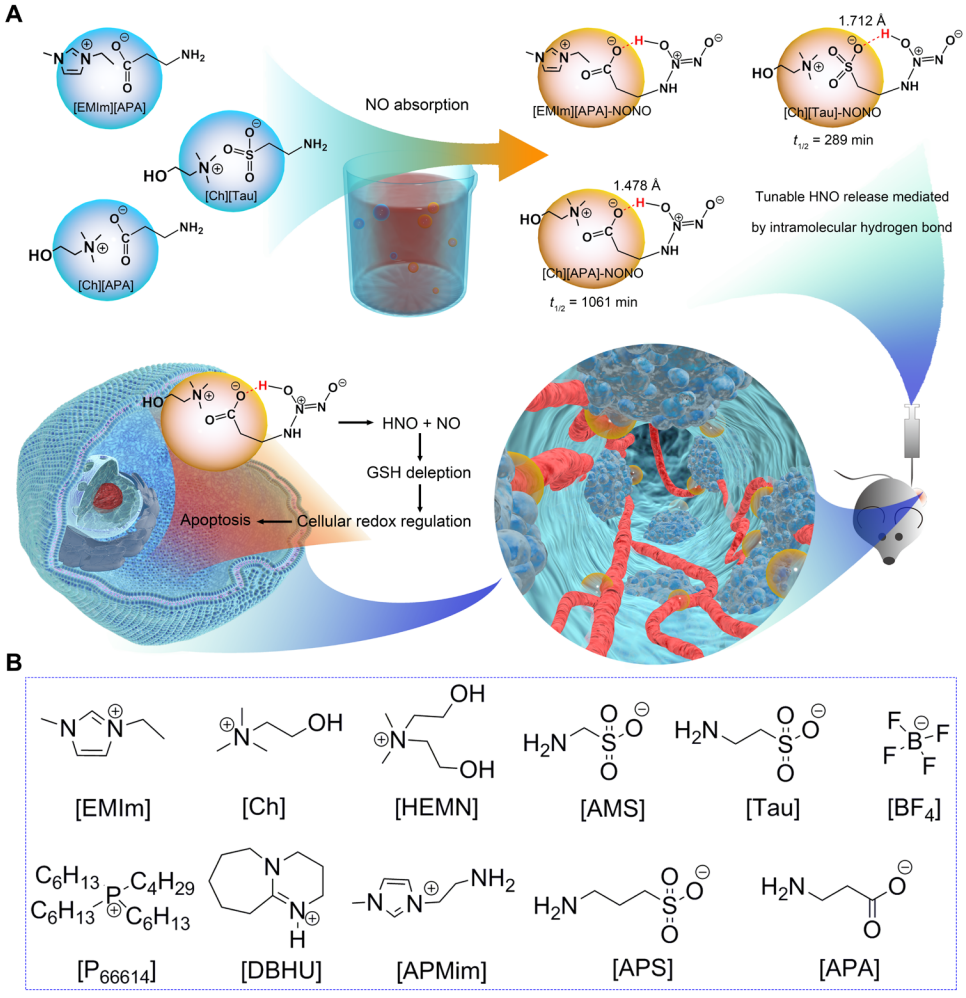

Fig. 1. A schematic illustration of the overall work design. (**A**) Schematic illustration of mechanisms for tunable release of HNO and tumor inhibition by IL-NONOates mediated by intramolecular hydrogen bond. (**B**) Structures of cations and anions used in this work. GSH, glutathione.

RESULTS

Synthesis and characterization of ILs

To construct the ILs for pharmacological application, anion and cation with high biocompatibility were first selected, such as taurine (Tau) and choline (Ch) (*30*). Our previous studies have proven that the basicity and chain length of ILs are important factors that govern their kinetics in gas absorption, which can be tuned by substituents on the anion (*2*). We thereby designed several primary amine-contained, anion-functionalized ILs (Fig. 1B), including [Ch][Tau], [HEMN][Tau], [DBU][Tau], [P_{66614}][Tau], [EMIm][Tau], [EMIm][AMS], [EMIm][APS], [EMIm][APA], and [Ch][APA].

A facile neutralization reaction was applied to prepare the ILs, by which the reaction between amino acid and phosphonium or imidazolium hydroxide in ethanol yielded the amino-functionalized ILs (*6*). The structures of these ILs were confirmed by nuclear magnetic resonance (NMR) spectroscopy (see the Supplementary Materials).

Absorption and release of NO by ILs

The traditional HNO donors were prepared under hyperbaric and alkalic conditions (*31*, *32*). Different from it, our IL-based HNO donors could be easily prepared by bubbling atmospheric NO into amino-functionalized ILs, forming IL-NONOates. NO absorption by ILs was investigated through gravimetric method at 30°C (Table 1 and Fig. 2A). The results indicated that the amino-functionalized ILs had high capacity of NO absorption and the absorption coefficient was higher than 2.0 mol of NO per mol IL. The UV-vis spectroscopic analysis revealed that the ─NONOate group within IL-NONOates induced a characteristic absorption at λ = 330 nm (Fig. 2B), which was notably different from that of other HNO donors (at about λ = 250 nm) (*33*). With the gradual decomposition of IL-NONOates, the characteristic absorption was attenuated and the captured NO was released. Accordingly, the attenuation of UV absorption at 330 nm could be used to indicate the dynamic process of NO release. By monitoring the UV absorption, the releasing kinetic curve was obtained, which suggested that the released NO was predominated by the form of HNO, accompanied by a small amount of NO (Fig. 2C). These IL-NONOates displayed obvious differences in the kinetics of HNO release. The $t_{1/2}$ were ranged from 211 to 1061 min for the IL-NONOates in phosphate-buffered saline (PBS) at pH 7.4 and 37°C (Table 1).

Effects of ILs structure on release

The comparison of $t_{1/2}$ among [Ch][Tau], [HEMN][Tau], [DBU][Tau], [P_{66614}][Tau], and [EMIm][Tau] indicated that the cation in

Table 1. NO absorption by amino-functionalized ILs and their releasing properties in PBS (pH 7.4) at 37°C.

Entry	IL	Absorption capacity*	$t_{1/2}$ (min)†
1	[Ch][Tau]	1.67	289
2	[HEMN][Tau]	2.51	242
3	[P_{66614}][Tau]	3.33	325
4	[DBU][Tau]	2.79	243
5	[EMIm][Tau]	2.28	211
6	[EMIm][AMS]	1.38	324
7	[EMIm][APS]	2.79	959
8	[EMIm][APA]	2.11	996
9	[Ch][APA]	1.70	1061
10	[APMim][BF4]	1.01	4.2

*The absorption was carried out at 30°C until full absorption, mol NO per mol of IL. †Determined at 37°C and pH 7.4 in 0.01 M phosphate buffer.

ILs had unobvious influence upon HNO release. With the same anion, ILs constructed with different cations displayed similar $t_{1/2}$. On the contrary, the anion played a crucial role in tuning the releasing rate. When the [Tau] was replaced by [APA], the $t_{1/2}$ of [Ch][APA] notably increased from 211 to 1061 min compared with that of [Ch][Tau]. We speculated that the intramolecular hydrogen bond was generated during the NO absorption, which induced the formation of IL-NONOates, and further regulated the HNO release kinetics. Thus, quantum chemical calculations were conducted to investigate the structure after NO absorption (*5*). Here, we selected [Tau]-NONO as an example. The geometry optimization of linear structure and hydrogen bond stabilized structure and energy gap between them were showed in Fig. 2D. After forming intramolecular hydrogen bond, **1b** was more stable than **1a** with linear structure, indicating that the hydrogen bond could stabilize its structure. Next, the UV-vis absorption of **1b** was predicted, and the obtained spectrum displayed a characteristic absorption of 326 nm. This result was consistent with our experimental result (330 nm) and further confirmed the intramolecular hydrogen bond–induced π-extension structure. Therefore, ascribed to the presence of hydrogen-bonding constraint, [Ch][Tau]-NONOate manifested a prolonged HNO release process as compared to the traditional HNO donors.

Given the fact that the $t_{1/2}$ of IL-NONOates was dramatically regulated by different anions, we believed that the anion affected the formation of intramolecular hydrogen bond by stabling proton in the —NONOate groups, and the strength of the hydrogen bond further mediated the $t_{1/2}$. Therefore, quantum chemical calculations for [Tau]-NONO, [AMS]-NONO, [APS]-NONO, and [APA]-NONO were performed (*34*), and the optimized geometries are shown in Fig. 2E. As expected, the interatomic distances between the O on sulfonyl carboxyl group or carboxyl group and the H on NONOate group were in the range of hydrogen bonding, which confirmed these anions forming intramolecular hydrogen bonds with NO absorption. In comparison with [Tau]-NONO, [AMS]-NONO, [APS]-NONO, and [APA]-NONO were calculated to have shorter interatomic distances at hydrogen bond sites, varying from 1.478 to 1.709 Å (Fig. 2E). The hydrogen bond distances of the IL-NONOates showed correlation with their $t_{1/2}$. For instance, the hydrogen bond distance of [Tau]-NONO was the longest and its $t_{1/2}$ was the shortest among these IL-NONOates, while [APA]-NONO had the shortest hydrogen bond distance accompanied by a prolonged HNO release (Fig. 2F). Since the distance of hydrogen bond reflected its bonding strength, the shorter hydrogen bonds resulted in the stronger intramolecular constraint, which stabilized the molecular geometry and increased the $t_{1/2}$.

Mechanism analysis

The intramolecular hydrogen bond in IL-NONOates was further investigated by Fourier transform infrared (FT-IR) spectroscopy (Fig. 3A). In the case of [Ch][Tau]-NONOate, the FT-IR spectrum displayed four new peaks at 876, 1217, 1353, and 1547 cm^{-1} compared with that of [Ch][Tau], which was derived from the formation of NONOates during NO absorption. Through a comparison with quantum chemical calculations and previous report (*6*), the peaks at 876 and 1353 cm^{-1} were mainly assigned to ν(N—N) in —NONOates, and additional peaks at 1217 and 1547 cm^{-1} were caused by ν(N—O) in —NONOates. By quantum chemical calculation, the predicted peaks of these vibration characteristics were located at 897, 1243, 1357, and 1524 cm^{-1}, respectively, which were close to the experimental results (Fig. 3D). Further NMR spectroscopic analysis revealed that chemical shifts at 12.77 and 5.23 parts per million (ppm) appeared in ^{1}H NMR spectrum of [Ch][Tau]-NONOate as compared to [Ch][Tau]; meanwhile, the chemical shifts at 38.3 and 54.5 ppm in ^{13}C NMR spectrum moved to 57.8 and 53.7 ppm, respectively. These variations were attributed to the formation of intramolecular hydrogen bond (Fig. 3, B, C, and E).

To further demonstrate the intramolecular hydrogen bond tuning, the $t_{1/2}$, 1-aminopropyl-3-methylimidazolium tetrafluoroborate IL [APMim][BF_4] was synthesized as a counterexample. [APMim][BF_4] left no room for formation of intramolecular hydrogen bond and was investigated for NO absorption and release. As shown in Table 1, [APMim][BF4]-based HNO donor exhibited a short $t_{1/2}$ of only 4.2 min, which highlighted that the HNO release behavior of IL-NONOates was substantially controlled by the formation and strength of intramolecular hydrogen bond.

On the basis of above results, we concluded that intramolecular hydrogen bonds were crucial to the tunability of IL-based HNO donor. By configuring the intramolecular hydrogen bond, the $t_{1/2}$ of HNO release could be flexibly adjusted for pharmacological applications.

The pharmacological potential of IL-NONOates

Given the versatile functions of reactive nitrogen species (RNS; here including HNO and NO) in physiological processes, the sustained and tunable HNO release property renders IL-NONOates with pharmacological potential as HNO donor. For malignant tumor, RNS production plays an alternative role by facilitating or inhibiting tumor progression (*35*). Notably, the RNS concentration is a main determinant for the alternative role in tumor. High RNS infiltrate has a propensity to react with thiols or thiol proteins, which leads to glutathione (GSH) depletion and redox alteration, consequently inducing tumor cell apoptosis (*22*, *36*). Accordingly, we believe that our IL-NONOates can serve as a HNO donor and steadily provide RNS within tumor, exerting an antitumor potential.

To validate the RNS supply of IL-NONOates in biological environment, decomposition of IL-NONOates was investigated in PBS and serous solutions [containing fetal bovine serum (FBS) and mouse serum]

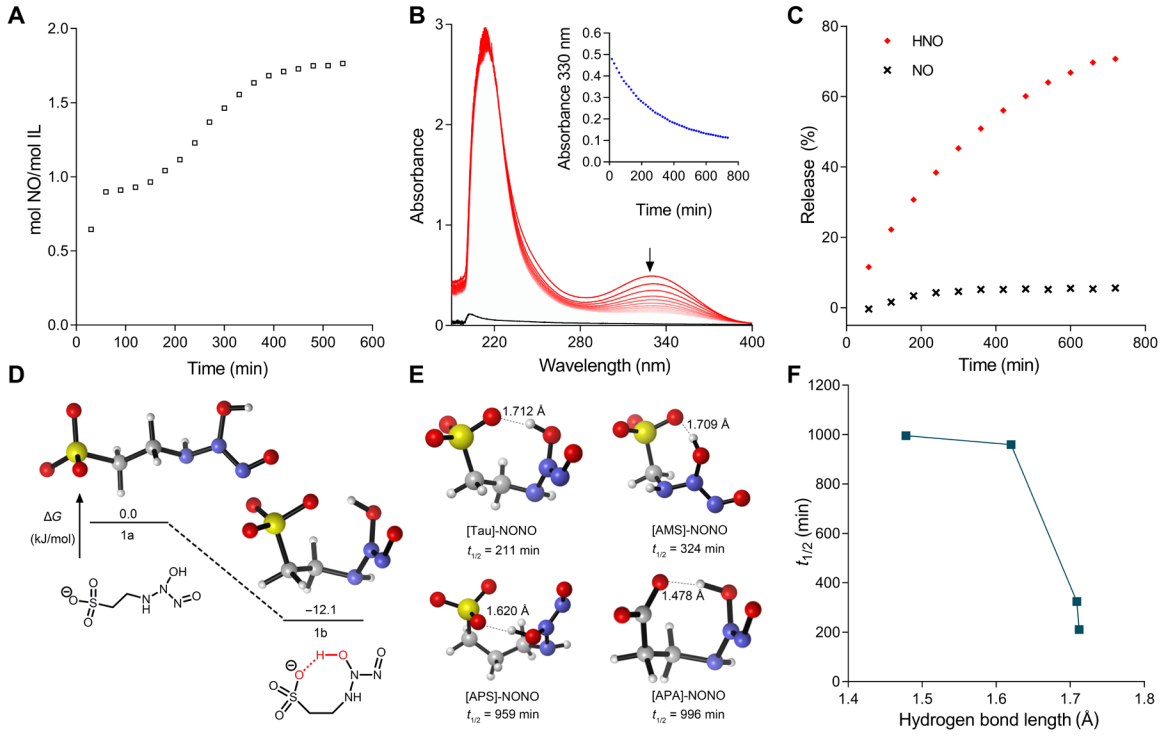

Fig. 2. The influence of intramolecular hydrogen bond on HNO-releasing $t_{1/2}$. (**A**) NO absorption by IL [Ch][Tau] at 30°C. (**B**) Spectrochemical monitoring of [Ch][Tau]-NONOate decomposition (red) was collected at 330 nm every 15 min (1-hour intervals shown) in PBS (pH 7.4) at 37°C. Spectrochemical of [Ch][Tau] in PBS (pH 7.4) at 37°C (black) has no absorption peak at 330 nm. Inset: Representative decay rates of [Ch][Tau]-NONOate. (**C**) Release kinetics of HNO and NO for [Ch][Tau]-NONOate in pH 7.4 PBS and at 37°C. (**D**) Energy gap between two different structures of [Tau]-NONO. (**E**) Optimized structures of [Tau]-NONO, [AMS]-NONO, [APS]-NONO, and [APA]-NONO. (**F**) Relationship between the lengths of intramolecular hydrogen bond and the $t_{1/2}$.

by monitoring the characteristic UV absorption at 330 nm. In Fig. 4A, the absorbances of IL-NONOates were gradually attenuated within 800 min, indicating the dynamic dissolution and HNO release. By calculating the $t_{1/2}$ (in table S1), we found that serous components slightly accelerated the releasing process, probably attributed to the interaction between IL-NONOates and serum albumins perturbing the intramolecular hydrogen bond within IL system. Obviously, [Ch][APA]-NONOate afforded slight effects due to the formation of stronger intramolecular hydrogen bonds. These results suggested that the IL-NONOates could achieve the sustained HNO release in simulated biological environment, which laid a foundation for further in vitro and in vivo investigations.

The in vitro antitumor effect of IL-NONOates was then investigated with tumor cell lines (CT-26 and MCF-7 cells). Before absorbing NO, pure ILs exhibited insignificant cytotoxicity upon tumor cells, indicating the biocompatibility of IL systems. After absorbing NO, IL-NONOates could efficiently induce cell death in a time- and dose-dependent manner (Fig. 4B and fig. S1). We speculated that the cytotoxicity was derived from the accumulation of intracellular RNS derived by IL-NONOates, so we analyzed the RNS level in the treated cells using red fluorescent dye reagent, and the cells treated with AS (a commercial HNO donor) were also examined as a positive control. After 4 hours of treatment, microscopic observation and flow cytometric quantification demonstrated that treatments with IL-NONOates afforded considerable amplification of intracellular RNS and the highest RNS induction was achieved by [Ch][APA]-NONOate, whereas AS failed to achieve this goal (Fig. 4C and fig. S2). To further interrogate the HNO-releasing process regulating the intracellular RNS, the relative RNS levels at 0.5 and 2 hours were analyzed by enzyme-linked immunosorbent assay (Fig. 4D). Treatment with [Ch][APA]-NONOate brought an accumulative increase in RNS level as compared to untreated control. In comparison, other treatments displayed relatively weaker RNS upregulations. The effective RNS induction of [Ch][APA]-NONOate consequently resulted in the GSH consumption in the treated cells (Fig. 4E). Treatments with [Ch][Tau]- and [EMIm][APA]-NONOates were also found to cause significant decreases in GSH. By contrast, a restoration of GSH was detected in the AS-treated cells because of AS lacking sustained HNO release capacity. The RNS amplication and redox dysregulation could trigger the programmed death for treated cells. The apoptosis results of CT-26 and MCF-7 cells by annexin V–fluorescein isothiocyanate (FITC)/propidium iodide (PI) staining indicated that IL-NONOates treatment could effectively induce apoptosis upon tumor cells (Fig. 4F and fig. S3). Although [Ch][APA]-NONOate had a longer $t_{1/2}$ of HNO release as compared to other IL-NONOates, it showed the highest intracellular RNS accumulation and the most efficient antitumor effect. We believed that the cell internalization was also a factor that affected the functionalization of IL-NONOates. To explore whether the cationic and anionic combination of ILs influenced the internalization, the binding constant between ILs and cardiolipin (CL) was measured by isothermal titration calorimetry (ITC). CL contained long hydrophobic alkyl chains and phosphate groups, which shared a similar molecular structure with phospholipid, the main component in cell membrane (*37*); thereby, the binding constant between ILs and CL could reflect the discrepancy in cell internalization. The titration

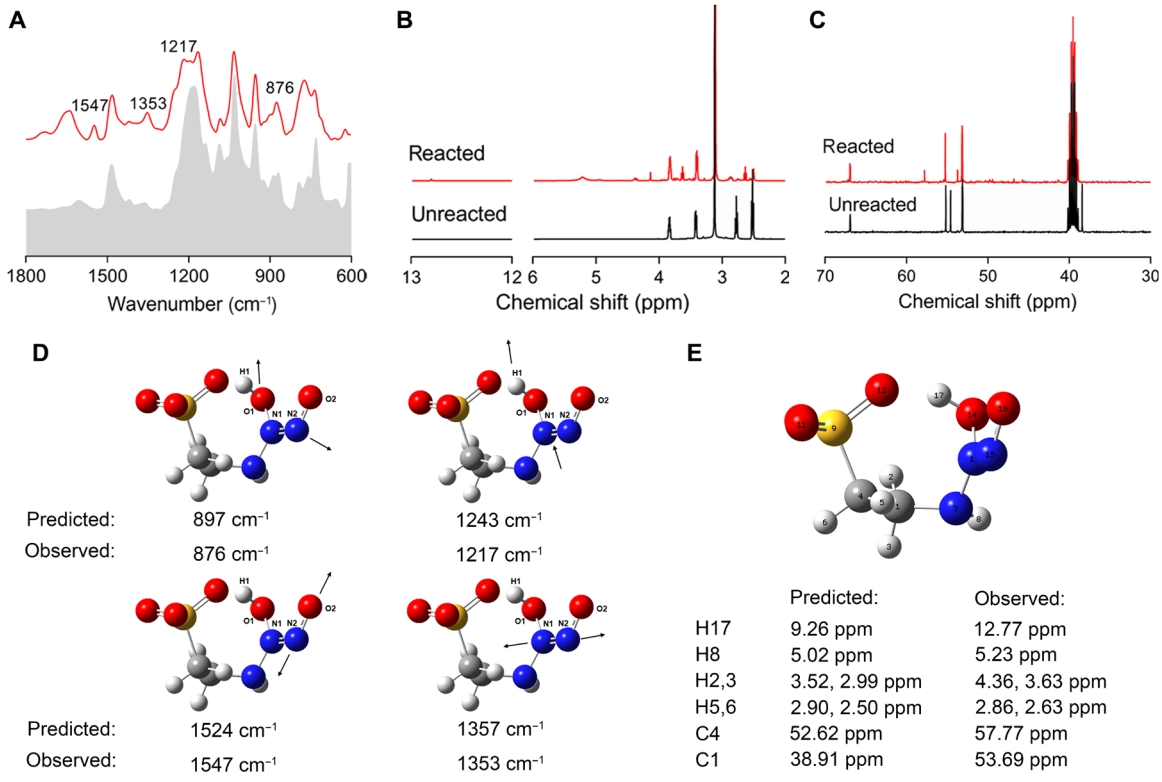

Fig. 3. The influence of intramolecular hydrogen bonds on spectroscopic investigations and quantum chemical calculations. (**A**) FT-IR. (**B**) ^{1}H NMR and (**C**) ^{13}C NMR spectra by IL [Ch][Tau] before and after NO absorption. (**D**) Prediction of vibration model for [Tau]-NONO. (**E**) Prediction of ^{1}H NMR and ^{13}C NMR spectra in [Tau]-NONO.

curves and thermodynamic analysis demonstrated that the binding constant of [Ch][APA] with CL was significantly higher than that of [Ch][Tau] or [EMIm][APA], which might facilitate the cell internalization of [Ch][APA] (fig. S4 and table S2).

Encouraged by the in vitro antitumor performance of IL-NONOates, we were keen to find out whether IL-NONOates had pharmacological potential to suppress tumor progression in vivo. CT-26 tumor model was established in BALB/c mice; then, the tumor-bearing mice were given with ILs and IL-NONOates three times a week via subcutaneous injection in tumor regions. During 22 days of treatment, tumor growth profiles indicated that the IL treatments had little suppression on malignant progression as compared to the control. Treatment with [Ch][Tau]-NONOate or [EMIm][APA]-NONOate moderately retards tumor growth (Fig. 5A and fig. S5), reducing the tumor volume to 80.7 and 78.2%, respectively. In the case of [Ch][APA]-NONOate, potent inhibiton on tumor growth was obtained and the tumor volume was only 44.7% to that of control (Fig. 5A). To investigate the mechanism underlying the effective tumor inhibiton for [Ch][APA]-NONOate, intratumoral RNS variation and GSH consumption after injection was evaluated using O52F fluorescence probe and 5,5′-dithiobis-(2-nitrobenzoic acid), respectively. Quantitative analysis revealed that the intratumoral RNS level was elevated in a time-dependent manner, and the RNS level at 8 hours after injection was 5.6 ± 1.4–fold higher than that of control (Fig. 5B). With the gradual increase in RNS, the intratumoral GSH was significantly down-regulated, showing obvious tendency of GSH depletion (Fig. 5C). These results validated that [Ch][APA]-NONOate could steadily provide RNS within tumor tissues, by which the intratumoral redox state was devastated, and the tumor cells lost their malignant or invasive abilities as a result of apoptosis. Tumor slices with immunohistochemical staining of terminal deoxynucleotidyl transferase–mediated deoxyuridine triphosphate nick end labeling (TUNEL) and Ki-67 substantiated that treatment with IL-NONOates could induce apoptosis and inhibit proliferation upon tumor cells; in particular, the strongest antitumor effect was achieved by [Ch][APA]-NONOate (Fig. 5D).

During treatment, IL-NONOates manifested good biosafety at the treated dose. Mice that received treatment displayed insignificant variations of body weight with survival rate above 30%. The examination of hemogram indexes showed negligible abnormities except for slight fluctuations in albumin and uric acid activities, confirming the biosafety of IL-NONOates (fig. S6).

DISCUSSION

Because of the intrinsic physicochemical properties, ILs have offered a highly tunable and reversible platform for absorption and separation of gases. In our previous works, we have designed various ILs with functionalized anions by flexible acid-base neutralization strategy to achieve efficient absorption and separation of gases including CO_2, SO_2, and NO_x (*2*, *4*, *6*). Mechanistically, these ILs captured and released gas through tunable chemical interactions with gas. This unique IL-gas system provided a new insight for developing IL drugs.

Here, we synthesized a series of ILs with different anions such as taurate for NO capture and HNO release and investigated their pharmacological potential using CT-26 tumor model. The ILs could capture NO by forming intramolecular hydrogen bond to

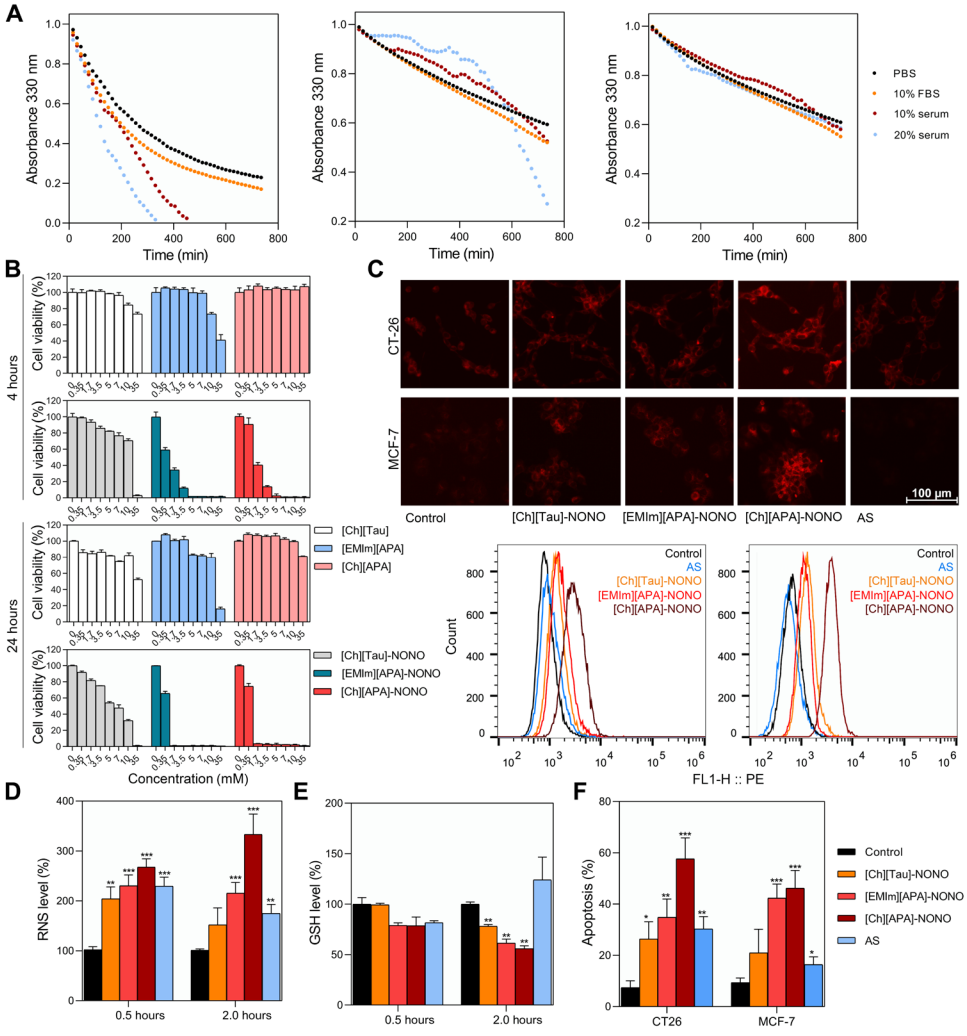

Fig. 4. IL-NONOates impair the growth of tumor cells by intracellularly accumulating RNS, depleting GSH, and inducing apoptosis. (**A**) Changes of representative decay rates of IL-NONOates were detected in simulated intracellular environment with fetal bovine serum (FBS) or mouse serum (serum), compared with PBS (pH 7.4) at 37°C. From left to right: [Ch][Tau]-NONOate, [EMIm][APA-NONOate, and [Ch][APA]-NONOate. (**B**) In vitro cytotoxicity of [Ch][Tau], [EMIm][APA], [Ch][APA], [Ch][Tau]-NONOate, [EMIm][APA]-NONOate, and [Ch][APA]-NONOate in CT-26 cells was evaluated after 4 or 24 hours of incubation with the sample by 3-(4,5-dimethylthiazol-2-yl)-2,5-diphenyltetrazolium bromide (MTT) assay ($n = 5$). (**C**) In vitro red fluorescence image of RNS production in CT-26 cells and MCF-7 cells treated with IL-NONOates or AS for 4 hours (scale bar, 100 μm). AS (a commercial HNO donor). (**D**) Quantification of intracellular RNS levels after 1.0 mM IL-NONOates treatments in CT-26 cells at indicated times ($n = 3$). (**E**) Quantification of intracellular GSH levels after 1.0 mM IL-NONOates treatments in CT-26 cells at indicated time points ($n = 3$). (**F**) Apoptosis of cells treated with IL-NONOates ($n = 3$). The error bars represented means ± SD. The *P* values were calculated by the Student's *t* test (*$P < 0.05$, **$P < 0.01$, and ***$P < 0.001$).

yield IL-NONOates, which was verified by UV-vis, IR, and NMR method (Fig. 3). Different from the weak influence of cation, the effect of the anion on the release of HNO was remarkable. Through optimizing the IL, the molecular interactions within IL-NONOates could be tuned to achieve a sustained HNO release with desired $t_{1/2}$, where strong intramolecular hydrogen bond resulted in the increased releasing $t_{1/2}$ (Fig. 2). Comparative analysis by experimental test and theoretical calculation indicated that the strength of intramolecular hydrogen bond was optimized in [Ch][APA]-NONOate system, enabling an idea HNO releasing kinetics ($t_{1/2}$, 1061 min) for pharmacological application, which is superior to traditional HNO donor (table S3). On the contrary, [APMim][BF_4]-based HNO donor in the absence of intramolecular hydrogen bond exhibited a short $t_{1/2}$ of only 4.2 min.

Given the biochemical nature of HNO, our IL-NONOates could act as a newly designed HNO donor for pharmacological application. Our study demonstrated that the IL-NONOates could permeate into tumor tissue and be internalized by tumor cells. With dynamic intracellular HNO releasing, IL-NONOates was evidenced to elevate RNS level and consume GSH content, leading to the alteration of redox homeostasis in vitro and in vivo. By regulating the redox state, the IL-NONOates effectively suppressed the survival of tumor cells, exerting a potent inhibition on malignancy (Fig. 5, A to C). These observations establish the possibility of using IL for efficient inhibition of tumor growth and point to the improvements that still need to be made to realize their full potential.

In conclusion, we have successfully designed a class of ILs using biocompatible molecules. Because of exquisite cation-anion combination

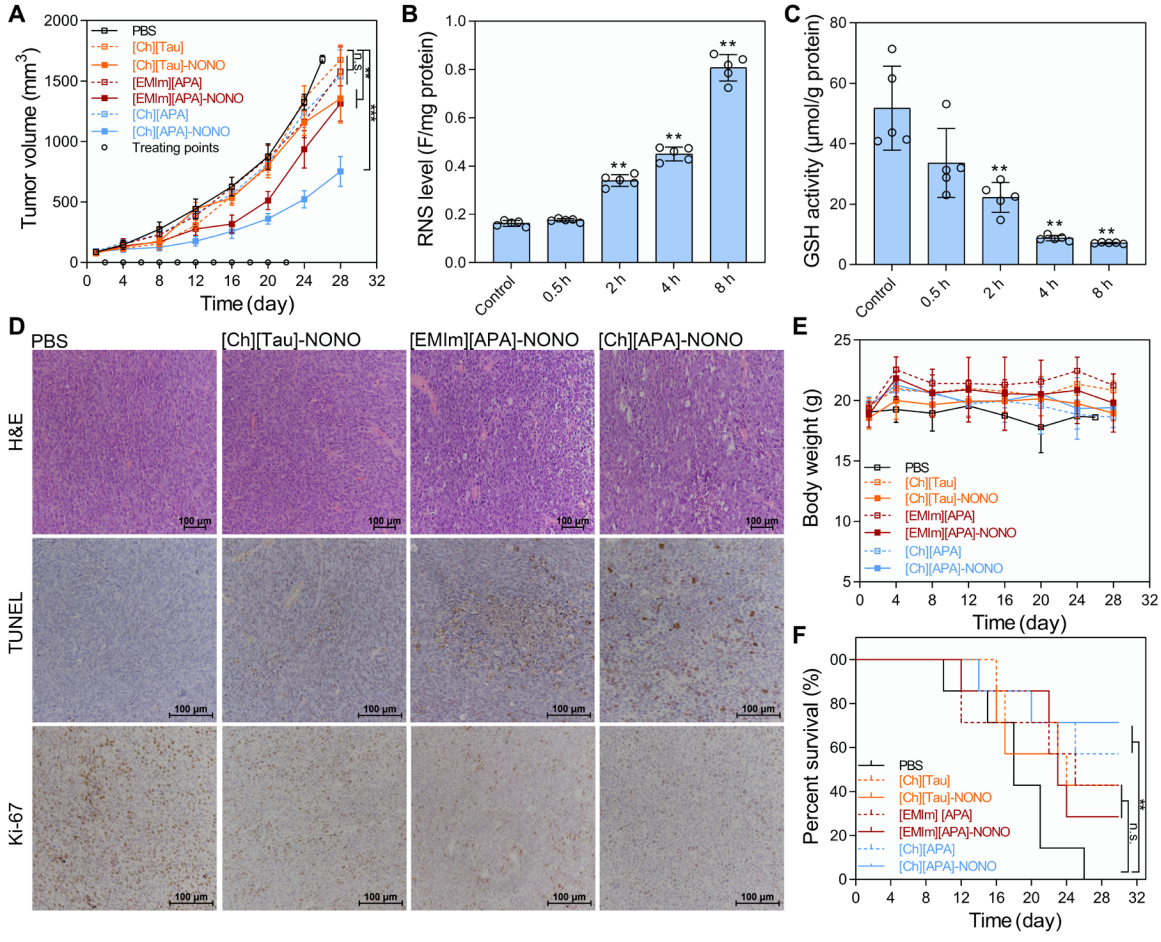

Fig. 5. IL-NONOates impair tumor growth and induce tumor regression. CT-26 tumor–bearing BALB/c mice were treated with PBS, [Ch][Tau], [EMIm][APA], [Ch][APA], [Ch][Tau]-NONOate, [EMIm][APA]-NONOate, and [Ch][APA]-NONOate. (**A**) Tumor volume (in mm^3) profile of treatment groups. The circle point (○) represented the day of treatment. (**B**) Quantitative analysis of intratumoral RNS levels. (**C**) Quantitative analysis of intratumoral GSH levels. The error bars represented means ± SD and $n = 7$. The *P* values were calculated by the Student's *t* test (n.s., no significance; $^{**}P < 0.01$ and $^{***}P < 0.001$). (**D**) Immunohistochemical analyses of hematoxylin and eosin (H&E), TUNEL, and Ki-67 for CT-26 tumor tissues from each group after treatments. (**E**) The average body weights of the treatment groups. (**F**) Kaplan-Meier survival curves of the treatment groups. The *P* values were calculated by the log-rank test ($n = 7$, $^{**}P < 0.01$).

and intramolecular hydrogen bond, these IL formulations can not only capture NO to form IL-NONOates but also release HNO in tunable kinetic processes. In vitro and in vivo studies have proven that the IL-NONOates effectively reverse the physiological redox through sustained HNO release and gradual GSH depletion, showing pharmacological potential in tumor inhibition. This innovative design based on chemical screening and hydrogen bond configuring has provided a new insight for IL drugs. Considering the versatile role of HNO in tumorigenesis and other diseases, our IL-NONOates have shown extensive application potential as a HNO donor in pharmaceuticals.

MATERIALS AND METHODS

Chemicals

All chemicals used in this work were purchased from commercial sources and used without further purification unless otherwise stated. Ch, bis (2-hydroxyethyl) dimethylammonium chloride ([HEMN][Cl]), 1,8-diazabicyclo[5.4.0]undec-7-ene (DBU), 1-ethyl-3-methylimidazolium bromide ([EMIm][Br]), aminomethanesulfonic acid (AMS), Tau, 3-amino-1-propanesulfonic acid (APS), and β-alanine (APA) were purchased from Energy-Chemistry Co. Ltd. Trihexyl (tetradecyl) phosphonium bromide ($[P_{66614}][Br]$) and $[APMim][BF_4]$ were obtained from J&K Scientific Ltd. AS ($Na_2N_2O_3$) was obtained from AmyJet Scientific Inc. NO (99.99%) and N_2 (99.99%) were purchased from Hangzhou Jingong Special Gas Co. Ltd. Cell culture products and 3-(4,5-dimethylthiazol-2-yl)-2,5-diphenyltetrazolium bromide (MTT) were purchased from Sigma-Aldrich (St. Louis, MO, USA). CL (18:1) was provided by Aladdin. Cellular ROS/RNS Detection Assay Kit and Annexin V–FITC Apoptosis Detection Kit were provided by Abcam. NO assay kit, RIPA lysis buffer, and GSH and oxidized GSH (GSSG) assay kit were bought from the Beyotime Institute of Biotechnology (Jiangsu, China). Tissular RNS assay kit and the GSH content assay kits were purchased from BestBio (Shanghai, China). Bicinchoninic acid (BCA) protein quantitation assay kit was purchased from KeyGenBio (Nanjing, China).

Absorption of NO by ILs

Before absorption, N_2 at a flow rate of 60 ml/min was used to drive air away from the experiment system, which would last 30 min. After that, NO of atmospheric pressure was bubbled through about 1 g of

IL in a glass container about 5 ml at a flow rate of about 20 ml/min. The glass container was partly immersed in a metal block at 30°C. The amount of NO absorbed was determined at regular intervals by an electronic balance with an accuracy of ±0.0001 g.

Quantum chemical calculations

All calculations were performed with Gaussian 09 package (*38*). Geometry optimizations and frequency calculations were carried out using the solvation model based on density (water) at the M062x/6-311++G (d, p) level. Each stationary point was confirmed by ensuring that there was no imaginary frequency. IR calculation was calculated by a self-consistent reaction field using the SMD (water) model at the M062x/6-311++G (d, p) level. NMR calculation was calculated by a self-consistent reaction field using the conductor-like polarizable continuum model (CPCM) [dimethyl sulfoxide (DMSO)] at the M062x/6-311++G (d, p) level.

Half-life determination studies for IL-NONOates

Half-lives of IL-NONOates were measured spectrophotometrically by monitoring the decrease in absorbance of the diazeniumdiolate chromophore at about 330-nm wavelength using a TU-1901 spectrophotometer. In a typical kinetic experiment, test compound was added to a buffer solution (0.01 mM PBS, pH 7.4). The final concentration of test compound was 1 mM. The sample was transferred to a UV cell for wavelength scanning within range from 190 to 400 nm at 37°C for 12 hours. The absorbance at each wavelength was recorded, and the overlapped absorbance was tacked to form a graphic illustrating the spectral changes accompanying the decomposition of test compound for various incubation times. The maximum absorbance at each time point was recorded to calculate the half-life. Absorbance time ($[A]_t$) data were obtained; then, first-order rate constants and $t_{1/2}$ were calculated using the following equations (*34*)

$$\ln [A]_t = -k\,t + \ln [A]_0$$

$$t_{1/2} = \ln 2/k$$

NO release from IL-NONOates

The IL-NONOates (1 mM) dissolved in PBS (pH 7.4) were incubated at 37°C from 0 to 12 hours, and NO was determined by quantification of nitrite using the Griess reaction. Nitrite was produced by the reaction of nitric oxide with oxygen and water. In this method, nitrite was first reacted with sulfanilamide in acidic media to form a transient diazonium salt. This intermediate was then allowed to react with *N*-naphthyl-ethylenediamine to form a stable azo compound that had a maximum absorbance at 540 nm. The absorbance of this adduct at 540 nm was linearly proportional to the nitrite concentration in the sample.

HNO release from IL-NONOates

The absorbance at 330-nm wavelength was proportional to the ─NONOate group concentration according to the Lambert-Beer law. The total amount of nitrogen released over a period of time could be calculated from the known initial concentration and initial absorbance. The amount of HNO released was indirectly determined by subtracting the amount of NO released, which was measured by Griess method, from the total amount of nitrogen released. Then, the percentage of HNO release was calculated by dividing the theoretical maximum HNO release.

Cell cultures

CT-26, MCF-7, and human embryonic kidney (HEK)–293 cell lines were purchased from the American Type Culture Collection (Rockville, MD). The MCF-7 and CT-26 were cultured in RPMI 1640 culture medium supplemented with 10% FBS, and HEK-293 cells were cultured in Dulbecco's modified Eagle medium supplemented with 10% FBS. The cells were cultured at 37°C in a humidified atmosphere containing 5% CO_2.

In vitro cytotoxicity study

The cytotoxicity of ILs and IL-NONOates were assessed by MTT assay. The CT-26, MCF-7, and HEK-293 cells were seeded in 96-well plates at a density of 10,000 cells per well for 18 hours. The culture medium was then replaced by serum-free media containing various concentrations of ILs and IL-NONOates. Next, the cells were incubated for 4, 8, 12, or 24 hours. Afterward, the media were removed and the cells were washed with PBS buffer; then, 100 μl of MTT solution (0.5 mg/ml) was added into each well. Four hours after MTT addition a volume of 100 μl of DMSO was added into each well to solubilize the formazan crystals and the absorbance of the formazan solution was measured at 570 nm using a spectrophotometer (Bio-Rad Model 680). All experiments were carried out with five replicates. The untreated cells served as the 100% cell viability control, and the completely dead cells served as the blank. The relative cell viability (%) related to control cells was calculated using the formula below

$$V\% = \frac{[A]_{\text{experiment}} - [A]_{\text{blank}}}{[A]_{\text{control}} - [A]_{\text{blank}}}$$

where V% is the percent of cell viability, $[A]_{\text{experimental}}$ is the absorbance of the wells culturing the treated cells, $[A]_{\text{blank}}$ is the absorbance of the blank, and $[A]_{\text{control}}$ is the absorbance of the wells culturing untreated cells.

Cell apoptosis assays

Apoptosis was measured by annexin V–FITC/PI double staining according to the apoptotic assay kit. MCF-7 and CT-26 cells cultured in 12-well plates were treated with IL-NONOates for 24 hours. The cells were digested and washed with PBS buffer. The collected cells were resuspended in 500 μl of binding buffer and stained with 5 μl of annexin V–FITC and 5 μl of PI for 15 min in the dark. The stained cells were analyzed by flow cytometry (BD FACSCalibur).

Cellular RNS detection

Intracellular RNS were detected using the Cellular ROS/RNS Detection Assay Kit. The CT-26, MCF-7, and HEK-293 cells cultured in 24-well plates were treated with the NO Detection Reagent using a volume sufficient to cover the cell monolayer. Then, the cells were incubated under normal tissue culture conditions for 2 hours. Afterward, the NO Detection Reagent was removed, and the cells were treated with ILs or IL-NONOates for 1, 2, or 4 hours. Next, ILs and IL-NONOates were removed, and the cells were washed once with 1× wash buffer. The cells were observed under an inverted fluorescence microscope with standard excitation/emission filter sets.

Cellular RNS and GSH quantitative analysis

The cells were seeded in 24-well plates at a density of 40,000 cells per well for 18 hours. The culture medium was then replaced by serum-free media containing various concentrations of IL-NONOates. After 0.5 or 2 hours of incubation, the cells were lysed and the intracellular RNS levels were quantified using RNS assay kit (Beyotime, China). The GSH levels were determined by GSH and GSSG assay kit (Beyotime, China).

ITC measurement

A VP-ITC (MicroCal) isothermal titration calorimeter was used to measure the binding interactions between ILs and 18:1 CL. Sample cell (V_{cell} = 1.4 ml) was filled with 18:1 CL aqueous solution. IL aqueous solution in a syringe was injected into CL aqueous solution (1 injection of 1 μl and 28 more injections of 5 μl each). The duration of each injection was 10 s, and the interval between each injection was 120 s. To ensure complete mixing in a few seconds, the injector stirred the aqueous solution at a rate of 1001 rpm. Calorimetric data were analyzed using Origin 7.0 software (MicroCal). The system temperature was set to 25°C (*37*).

Tumor model

Male BALB/c mice (6 weeks old, ~20 g) were purchased from Zhejiang Academy of Medical Sciences and maintained in a pathogen-free environment under controlled temperature. Animal care and handing procedures were in accordance with the guidelines approved by the ethics committee of Zhejiang University. All study protocols involving animals were approved by the Zhejiang University Animal Care and Use Committee (ZJU20190025). The mice were injected subcutaneously in the right flank region with 200 μl of cell suspension containing 4×10^6 CT-26 cells. The tumors were allowed to grow to ~100 mm^3 before experimentation. The tumor volume was calculated as (tumor length) × $(\text{tumor width})^2/2$.

In vivo cancer treatment on tumor models

CT-26 tumor–bearing mice were randomly divided into seven groups (n = 7). When the mean tumor volume reached ~100 mm^3 (set as day 1), mice received different treatments via subcutaneous injection: control, [Ch][Tau], [EMIm][APA], [Ch][APA], [Ch][Tau]-NONOate, [EMIm][APA]-NONOate, and [Ch][APA]-NONOate (5 μmol per mice). The treatment lasted for 22 days. During the treatment, tumor volume and body weight of the treated mice were measured every 2 days using a caliper and an electronic balance, respectively.

Intratumoral RNS levels detection

Fifty milligrams of fresh tumor tissue was made into homogenate with 1 ml of buffer. Then, the supernatants for RNS determination were obtained by centrifugation at 4°C for 10 min. RNS levels were detected using an RNS assay kit (BestBio, China). Meanwhile, the total protein contents were quantified by the BCA protein quantitation assay kit (KeyGenBio, China). All samples were repeated in triplicate. The levels of RNS were expressed in F/mg protein.

Intratumoral GSH activities detection

The tumor tissue was quick-frozen with liquid nitrogen and was quickly mashed. Then, protein precipitation working fluid was added into the tissue homogenates. Then, the homogenates were incubated at 4°C for 10 min and were centrifuged at 10,000*g* for 10 min. The supernatants were obtained for GSH determination. The activities of GSH were detected using kits (BestBio, China), and the total protein contents were quantified using a BCA protein quantitation assay kit (KeyGenBio, China). All samples were repeated in triplicate. The levels of GSH were expressed in μmol/g protein.

In vivo biosafety

Male BALB/c mice were randomly divided into seven groups (four for each group). The mice were subcutaneously injected with PBS, [Ch][Tau], [EMIm][APA], [Ch][APA], [Ch][Tau]-NONOate, [EMIm][APA]-NONOate, and [Ch][APA]-NONOate at the dosage of 5 μmol per mice. After 24 hours, the mice were anesthetized and the blood was collected. The blood samples were analyzed using an automatic biochemical parameter analyzer (Hitachi 7020, Japan) to evaluate the liver/kidney function–related indicators, including total protein, alkaline phosphatase, albumin, alanine aminotransferase, creatinine, blood urea nitrogen, and uric acid.

Immunohistochemistry

For the histological assay, the tumor tissues were fixed in 4% paraformaldehyde for 48 hours. The specimens were then dehydrated in graded ethanol, embedded in paraffin, and cut into 5-mm-thick sections. The fixed sections were deparaffinized and hydrated according to a standard protocol and stained with hematoxylin and eosin for microscopic observation. For the analysis of cell proliferation, the sections were incubated with anti–Ki-67 antibody (1:25; ab28364, Abcam, UK) and were then incubated with a secondary antibody of a rabbit IgG (H + L)/HRP (ZB-2301, ZSGB-BIO, China) according to the manufacturer's instructions. Apoptosis of tumor cells following treatments in the mice was determined using the TUNEL method according to the manufacturer's instructions (Roche, Basel, Switzerland). All the sections were examined on an inverted fluorescence microscopy (Olympus, IX71).

Statistical analysis

All the experiments were repeated at least three times, and the data were presented as means and SD. The statistical significance was evaluated by the Student's t test when only two groups were compared.

SUPPLEMENTARY MATERIALS

Supplementary material for this article is available at http://advances.sciencemag.org/cgi/content/full/6/45/eabb7788/DC1

View/request a protocol for this paper from *Bio-protocol*.

REFERENCES AND NOTES

1. J. L. Shamshina, S. P. Kelley, G. Gurau, R. D. Rogers, Chemistry: Develop ionic liquid drugs. *Nature* **528**, 188–189 (2015).
2. C. Wang, X. Luo, H. Luo, D. Jiang, H. Li, S. Dai, Tuning the basicity of ionic liquids for equimolar CO_2 capture. *Angew. Chem. Int. Ed. Engl.* **50**, 4918–4922 (2011).
3. N. K. Vishwakarma, A. K. Singh, Y.-H. Hwang, D.-H. Ko, J.-O. Kim, A. G. Babu, D.-P. Kim, Integrated CO_2 capture-fixation chemistry via interfacial ionic liquid catalyst in laminar gas/liquid flow. *Nat. Commun.* **8**, 14676 (2017).
4. C. Wang, G. Cui, X. Luo, Y. Xu, H. Li, S. Dai, Highly efficient and reversible SO_2 capture by tunable azole-based ionic liquids through multiple-site chemical absorption. *J. Am. Chem. Soc.* **133**, 11916–11919 (2011).
5. D.-J. Tao, F.-F. Chen, Z.-Q. Tian, K. Huang, S. M. Mahurin, D. Jiang, S. Dai, Highly efficient carbon monoxide capture by carbanion-functionalized ionic liquids through C-site interactions. *Angew. Chem. Int. Edit.* **56**, 6843–6847 (2017).
6. K. Chen, G. Shi, X. Zhou, H. Li, C. Wang, Highly efficient nitric oxide capture by azole-based ionic liquids through multiple-site absorption. *Angew. Chem. Int. Edit.* **55**, 14362–14366 (2016).

7. D. M. Piper, T. Evans, K. Leung, T. Watkins, J. Olson, S. C. Kim, S. S. Han, V. Bhat, K. H. Oh, D. A. Buttry, S. H. Lee, Stable silicon-ionic liquid interface for next-generation lithium-ion batteries. *Nat. Commun.* **6**, 6230 (2015).
8. S. Bai, P. Da, C. Li, Z. Wang, Z. Yuan, F. Fu, M. Kawecki, X. Liu, N. Sakai, J. T.-W. Wang, S. Huettner, S. Buecheler, M. Fahlman, F. Gao, H. J. Snaith, Planar perovskite solar cells with long-term stability using ionic liquid additives. *Nature* **571**, 245–250 (2019).
9. B. A. Rosen, A. Salehi-Khojin, M. R. Thorson, W. Zhu, D. T. Whipple, P. J. A. Kenis, R. I. Masel, Ionic liquid–mediated selective conversion of CO_2 to CO at low overpotentials. *Science* **334**, 643–644 (2011).
10. Y. Ren, J. Guo, Z. Liu, Z. Sun, Y. Wu, L. Liu, F. Yang, Ionic liquid–based click-ionogels. *Sci. Adv.* **5**, eaax0648 (2019).
11. K. S. Egorova, E. G. Gordeev, V. P. Ananikov, Biological activity of ionic liquids and their application in pharmaceutics and medicine. *Chem. Rev.* **117**, 7132–7189 (2017).
12. W. L. Hough, M. Smiglak, H. Rodríguez, R. P. Swatloski, S. K. Spear, D. T. Daly, J. Pernak, J. E. Grisel, R. D. Carliss, M. D. Soutullo, J. H. Davis Jr., R. D. Rogers, The third evolution of ionic liquids: Active pharmaceutical ingredients. *New J. Chem.* **31**, 1429–1436 (2007).
13. I. C. B. Martins, M. C. Oliveira, H. P. Diogo, L. C. Branco, M. T. Duarte, Mechano API-ILs: Pharmaceutical ionic liquids obtained through mechanochemical synthesis. *ChemSusChem* **10**, 1360–1363 (2017).
14. H. Wang, G. Gurau, J. Shamshina, O. A. Cojocaru, J. Janikowski, D. R. MacFarlane, J. H. Davis Jr., R. D. Rogers, Simultaneous membrane transport of two active pharmaceutical ingredients by charge assisted hydrogen bond complex formation. *Chem. Sci.* **5**, 3449–3456 (2014).
15. O. Zavgorodnya, J. L. Shamshina, M. Mittenthal, P. D. McCrary, G. P. Rachiero, H. M. Titi, R. D. Rogers, Polyethylene glycol derivatization of the non-active ion in active pharmaceutical ingredient ionic liquids enhances transdermal delivery. *New J. Chem.* **41**, 1499–1508 (2017).
16. Y. Miwa, H. Hamamoto, T. Ishida, Lidocaine self-sacrificially improves the skin permeation of the acidic and poorly water-soluble drug etodolac via its transformation into an ionic liquid. *Eur. J. Pharm. Biopharm.* **102**, 92–100 (2016).
17. L. J. Ignarro, Nitric oxide: A unique endogenous signaling molecule in vascular biology (Nobel lecture). *Angew. Chem. Int. Ed.* **38**, 1882–1892 (1999).
18. E. Culotta, D. E. Koshland Jr., No news is good news. *Science* **258**, 1862–1865 (1992).
19. A. W. Carpenter, M. H. Schoenfisch, Nitric oxide release: Part II. Therapeutic applications. *Chem. Soc. Rev.* **41**, 3742–3752 (2012).
20. R. F. Furchgott, Endothelium-derived relaxing factor: Discovery, early studies, and identifcation as nitric oxide (Nobel lecture). *Angew. Chem. Int. Ed.* **38**, 1870–1880 (1999).
21. F. Murad, Discovery of some of the biological effects of nitric oxide and its role in cell signaling (Nobel lecture). *Angew. Chem. Int. Ed.* **38**, 1857–1868 (1999).
22. P. Pagliaro, D. Mancardi, R. Rastaldo, C. Penna, D. Gattullo, K. M. Miranda, M. Feelisch, D. A. Wink, D. A. Kass, N. Paolocci, Nitroxyl affords thiol-sensitive myocardial protective effects akin to early preconditioning. *Free Radical Biol. Med.* **34**, 33–43 (2003).
23. L. K. Keefer, Fifty years of diazeniumdiolate research. From laboratory curiosity to broad-spectrum biomedical advances. *ACS Chem. Biol.* **6**, 1147–1155 (2011).
24. N. Paolocci, M. I. Jackson, B. E. Lopez, K. Miranda, C. G. Tocchetti, D. A. Wink, A. J. Hobbs, J. M. Fukuto, The pharmacology of nitroxyl (HNO) and its therapeutic potential: Not just the Janus face of NO. *Pharmacol. Ther.* **113**, 442–458 (2007).
25. K. M. Miranda, H. T. Nagasawa, J. P. Toscano, Donors of HNO. *Curr. Top. Med. Chem.* **5**, 649–664 (2005).
26. K. M. Miranda, T. Katori, C. L. T. de Holding, L. Thomas, L. A. Ridnour, W. J. McLendon, S. M. Cologna, A. S. Dutton, H. C. Champion, D. Mancardi, C. G. Tocchetti, J. E. Saavedra, L. K. Keefer, K. N. Houk, J. M. Fukuto, D. A. Kass, N. Paolocci, D. A. Wink, Comparison of the NO and HNO donating properties of diazeniumdiolates: Primary amine adducts release HNO in vivo. *J. Med. Chem.* **48**, 8220–8228 (2005).
27. A. S. Dutton, J. M. Fukuto, K. N. Houk, Mechanisms of HNO and NO production from Angeli's salt: Density functional and CBS-QB3 theory predictions. *J. Am. Chem. Soc.* **126**, 3795–3800 (2004).
28. D. J. Salmon, C. L. T. de Holding, L. Thomas, K. V. Peterson, G. P. Goodman, J. E. Saayedra, A. Srinivasan, K. M. Davies, L. K. Keefer, K. M. Miranda, HNO and NO release from a primary amine-based diazeniumdiolate as a function of pH. *Inorg. Chem.* **50**, 3262–3270 (2011).
29. C. M. Maragos, D. Morley, D. A. Wink, T. M. Dunams, J. E. Saavedra, A. Hoffman, A. A. Bove, L. Isaac, J. A. Hrabie, L. K. Keefer, Complexes of No with nucleophiles as agents for the controlled biological release of nitric-oxide. vasorelaxant effects. *J. Med. Chem.* **34**, 3242–3247 (1991).
30. S. Schaffer, H. W. Kim, Effects and mechanisms of taurine as a therapeutic agent. *Biomol. Ther.* **26**, 225–241 (2018).
31. R. S. Drago, B. R. Karstetter, The reaction of nitrogen(II) oxide with various primary and secondary amines. *J. Am. Chem. Soc.* **83**, 1819–1822 (1961).
32. R. S. Drago, F. E. Paulik, The reaction of nitrogen (II) oxide with diethylamine. *J. Am. Chem. Soc.* **82**, 96–98 (1960).
33. Z. J. Huang, J. Kaur, A. Bhardwaj, N. Alsaleh, J. A. Reisz, J. F. DuMond, S. B. King, J. M. Seubert, Y. H. Zhang, E. E. Knaus, O^2-sulfonylethyl protected isopropylamine diazen-1-ium-1,2-diolates as nitroxyl (HNO) donors: Synthesis, β-elimination fragmentation, HNO release, positive inotropic properties, and blood pressure lowering studies. *J. Med. Chem.* **55**, 10262–10271 (2012).
34. E. Espinosa, E. Molins, C. Lecomte, Hydrogen bond strengths revealed by topological analyses of experimentally observed electron densities. *Chem. Phys. Lett.* **285**, 170–173 (1998).
35. D. Fukumura, S. Kashiwagi, R. K. Jain, The role of nitric oxide in tumour progression. *Nat. Rev. Cancer* **6**, 521–534 (2006).
36. P. K. Lala, C. Chakraborty, Role of nitric oxide in carcinogenesis and tumour progression. *Lancet Oncol.* **2**, 149–156 (2001).
37. H. Fang, Z. Guo, L. Lin, J. Chen, P. Sun, J. Wu, C. Xu, H. Tian, X. Chen, Molecular strings significantly improved the gene transfection efficiency of polycations. *J. Am. Chem. Soc.* **140**, 11992–12000 (2018).
38. M. J. Frisch, G. W. Trucks, H. B. Schlegel, G. E. Scuseria, M. A. Robb, J. R. Cheeseman, G. Scalmani, V. Barone, B. Mennucci, G. A. Petersson, H. Nakatsuji, M. Caricato, X. Li, H. P. Hratchian, A. F. Izmaylov, J. Bloino, G. Zheng, J. L. Sonnenberg, M. Hada, M. Ehara, K. Toyota, R. Fukuda, J. Hasegawa, M. Ishida, T. Nakajima, Y. Honda, O. Kitao, H. Nakai, T. Vrevessn, J. A. Montgomery, Jr., J. E. Peralta, F. Ogliaro, M. Bearpark, J. J. Heyd, E. Brothers, K. N. Kudin, V. N. Staroverov, R. Kobayashi, J. Normand, K. Raghavachari, A. Rendell, J. C. Burant, S. S. Iyengar, J. Tomasi, M. Cossi, N. Rega, J. M. Millam, M. Klene, J. E. Knox, J. B. Cross, V. Bakken, C. Adamo, J. Jaramillo, R. Gomperts,R. E. Stratmann, O. Yazyev, A. J. Austin, R. Cammi, C. Pomelli, J. W. Ochterski, R. L. Martin, K. Morokuma, V. G. Zakrzewski, G. A. Voth, P. Salvador, J. J. Dannenberg, S. Dapprich, A. D. Daniels, O. Farkas, J. B. Foresman, J. V. Ortiz, J. Cioslowski, D. J. Fox, *Gaussian 09, Revision* $_{D.01}$ (Gaussian, Inc., 2009).
39. F. T. Bonner, Y. Ko, Kinetic, isotopic, and nitrogen-15 NMR study of N-hydroxybenzenesulfonamide decomposition: An nitrosyl hydride (HNO) source reaction. *Inorg. Chem.* **31**, 2514–2519 (1992).
40. X. Sha, T. S. Isbell, R. P. Patel, C. S. Day, S. B. King, Hydrolysis of acyloxy nitroso compounds yields nitroxyl (HNO). *J. Am. Chem. Soc.* **128**, 9687–9692 (2006).

Acknowledgments

Funding: This work was primarily funded by the National Natural Science Foundation of China (21776239), the Zhejiang Provincial Natural Science Foundation of China (LZ17B060001), and the Fundamental Research Funds of the Central Universities. **Author contributions:** The experimental strategy was proposed initially by C.W. and developed by all authors. Experiments were performed by X.L., K.C., and H.B. C.W. wrote the manuscript, with input from all co-authors. **Competing interests:** The authors declare that they have no competing interests. **Data and materials availability:** All data needed to evaluate the conclusions in the paper are present in the paper and/or the Supplementary Materials. Additional data related to this paper may be requested from the authors.

Submitted 18 March 2020
Accepted 23 September 2020
Published 6 November 2020
10.1126/sciadv.abb7788

Citation: X. Lv, K. Chen, G. Shi, W. Lin, H. Bai, H. Li, G. Tang, C. Wang, Design and tuning of ionic liquid–based HNO donor through intramolecular hydrogen bond for efficient inhibition of tumor growth. *Sci. Adv.* **6**, eabb7788 (2020).